Effective theory of the $\Delta(1232)$ resonance in Compton scattering off the nucleon

Vladimir Pascalutsa* and Daniel R. Phillips†
Department of Physics and Astronomy, Ohio University, Athens, Ohio 45701
(Received 4 December 2002; published 7 May 2003)

We formulate a new power-counting scheme for a chiral effective-field theory of nucleons, pions, and Δs. This extends chiral perturbation theory into the Δ-resonance region. We calculate nucleon Compton scattering up to next-to-leading order in this theory. The resultant description of existing γp cross-section data is very good for photon energies up to about 300 MeV. We also find reasonable numbers for the spin-independent polarizabilities α_p and β_p.

DOI: 10.1103/PhysRevC.67.055202 PACS number(s): 14.20.Dh, 12.39.Fe, 13.60.Fz, 25.20.Dc

I. INTRODUCTION

Compton scattering on the proton (γp) and the deuteron (γD) provides a clean and unique probe of nucleon electromagnetic structure, revealing information different to that obtained in electron scattering. During the last decade a number of excellent experimental programs have been dedicated to these two processes (see Refs. [1–5] and [6–10], respectively). At low photon energies, these experiments probe the static properties of the nucleon, such as its electric charge, magnetic moment, and polarizabilities. Above the pion-production threshold, the process becomes dominated by the excitation of resonances, most prominently the $\Delta(1232)$ isobar. Many theoretical methods aim at understanding this process in both the low-energy and the resonance region. In particular, significant progress has been made recently using dispersion relations [11,12] and effective Lagrangian models [13–15]. On the other hand, previous calculations using chiral perturbation theory (χPT) appear to work only at low photon energies—energies at or below the pion-production threshold [16,17]. This present study attempts to extend these χPT calculations above the pion threshold and into the Δ-resonance region.

In the low-energy regime, χPT seems to work extremely well. At next-to-leading order (NLO), i.e., third order in small momenta [$=O(q^3)$], heavy-baryon (HB) χPT for the electric and magnetic polarizabilities predicts [18,19]:

$$\alpha_p=\alpha_n=\frac{5\pi\alpha}{6m_\pi}\left(\frac{g_A}{4\pi f_\pi}\right)^2=12.2\times10^{-4}\ \text{fm}^3, \tag{1}$$

$$\beta_p=\beta_n=\frac{\pi\alpha}{12m_\pi}\left(\frac{g_A}{4\pi f_\pi}\right)^2=1.2\times10^{-4}\ \text{fm}^3, \tag{2}$$

where $\alpha=e^2/4\pi\simeq1/137$, $g_A\simeq1.26$, $f_\pi\simeq93$ MeV, and $m_\pi\simeq139$ MeV.[1] Since there are no Compton counterterms present at $O(q^3)$, this is a genuine prediction of χPT—a prediction which, at least for the proton, is in remarkable agreement with recent extractions of these quantities from low-energy data, e.g., Ref. [20]:

$$\alpha_p=(12.1\pm1.1\pm0.5)\times10^{-4}\ \text{fm}^3, \tag{3}$$

$$\beta_p=(3.2\pm1.1\pm0.1)\times10^{-4}\ \text{fm}^3. \tag{4}$$

Here the first error is statistical, and the second one represents the theory error of the fit to data.

However, the agreement of the NLO HBχPT prediction with the experimental γp cross-section data is good only up to photon energies $\omega\simeq100$ MeV [16]. The recent NNLO [$O(q^4)$] calculation [17] agrees with experiment to slightly higher energies, but above $\omega\simeq120$ MeV significant discrepancies begin to appear, most notably at backward angles. This is perhaps not surprising, since the Δ-isobar excitation is not included explicitly in this chiral expansion. And, as we shall argue, the breakdown scale of χPT without an explicit Δ is set essentially by the Δ-nucleon mass difference:

$$\Delta\equiv M_\Delta-M_N\approx293\ \text{MeV}. \tag{5}$$

Thus, to extend the region of χPT applicability to $\omega\sim\Delta$, the Δ must be included as an explicit degree of freedom.

The Δ contribution for the Compton amplitude had already been analyzed using chiral effective Lagrangians with explicit Δs in Refs. [21–23]. These studies focused mainly on nucleon polarizabilities. The predictions made in Refs. [19,21,22] are obscured by off-shell ambiguities, in particular by the so-called *off-shell parameters* that control the infamous spin-1/2 sector of the spin-3/2 Δ field. In a ''reasonable'' range for these parameters the Δ contribution to $\beta_p^{(\Delta)}$ varies between 0 and 14×10^{-4}fm^3 [22]. In contrast, Hemmert *et al.* [23], to next-to-leading order in their *small scale expansion* (SSE) [24], found a result which was independent

*Email address: vlad@phy.ohiou.edu
†Email address: phillips@phy.ohiou.edu

[1]Throughout this paper the designations LO, NLO, etc. refer to the order in the γN amplitude. These one-loop results are, strictly speaking, *leading-order* predictions for α_p and β_p, but we refer to them as next-to-leading order (NLO) since Eq. (1) is derived by considering the NLO result for the nucleon Compton amplitude.

of the off-shell parameters, and thus is apparently a reliable prediction. But this prediction for the Δ contribution to the magnetic polarizability is $\beta_p^{(\Delta)} \approx 9\times 10^{-4}$ fm^3, in dramatic contradiction with experiment [25]. (For an attempt to remedy this using a ''modified SSE,'' see Ref. [26].)

In this work we include the Δ in the chiral Lagrangian in a fashion somewhat different to this literature. First of all, the Lagrangian is written such that the unphysical spin-1/2 components of the Δ field decouple from observables [27,28], hence no off-shell parameters appear. This feature of our Lagrangian, besides removing the redundant parameters, allows us to dress the Δ-pole contribution in a manifestly covariant way.

Furthermore, we set up our power-counting scheme so that it is both closely connected to the usual χPT without explicit Δs in the low-energy region $\omega \sim m_\pi$, *and* extends to the Δ region $\omega \sim \Delta$. This is achieved by recognizing the hierarchy of scales:

$$m_\pi \ll \Delta \ll \Lambda \sim 1 \text{ GeV}, \tag{6}$$

where Λ stands for the ''high-energy scale,'' the breakdown scale of the theory. Therefore, our scheme is rather different from the SSE of Refs. [23,24] (see also Ref. [29]), where the Δ-nucleon mass difference is assumed to be of order m_π (i.e., $\Delta \sim m_\pi$). A more detailed comparison of our scheme and the SSE will be given below.

With the three-scale hierarchy (6), one in principle has two small expansion parameters: m_π/Δ and Δ/Λ. We regard both of them as roughly the same size, and so introduce a single small parameter:

$$\delta = \frac{\Delta}{\Lambda} \sim \frac{m_\pi}{\Delta}. \tag{7}$$

Note that this implies that m_π scales as δ^2.

The validity of the scale hierarchy (6) and the expansion in powers of δ (which we shall refer to as the δ *expansion*) is to be judged by the success of the resultant effective-field-theory (EFT) description of processes involving the excitation of Δ. We regard the results we shall present here for γp scattering as significant evidence in favor of this EFT expansion.

To obtain the NLO result for γN scattering in our scheme for both the low-energy and the Δ regions, the Δ-pole contribution to this process must be dressed, and then added to the NLO HBχPT result. This introduces two free parameters that characterize the strength of the $\gamma N \to \Delta$ transition, g_M and g_E. Adjusting these parameters we find very good agreement with the experimental γp differential cross section up to $\omega \approx 300$ MeV, thereby extending the domain of applicability of chiral EFT into the Δ region. At the same time we also find reasonable values for the nucleon polarizabilities.

In the following section we introduce the Lagrangian for the Δ and discuss its properties. Section III then describes the δ expansion for Compton scattering on the proton. In particular, we show that for $\omega \sim m_\pi$ the power counting is very similar to that of HBχPT, while for $\omega \sim \Delta$ the power counting mandates resummation of the Δ propagator, thereby dressing the Δ and giving it a finite width. In Sec. IV we summarize the elements of our calculation, and then in Sec. V we present and discuss the results of our NLO calculation for the differential cross section, as well as for the spin-independent polarizabilities α_p, β_p. We conclude in Sec. VI.

II. THE CHIRAL LAGRANGIAN

The pion-nucleon sector of the HBχPT Lagrangian is well discussed in the literature, see e.g., Ref. [19]. The terms relevant for our purposes are[2]

$$\begin{aligned}\mathcal{L} = {} & \tfrac{1}{2} D_\mu^{ab} \pi_a D^{\mu bc} \pi_c - \tfrac{1}{2} m_\pi^2 \pi^2 + \overline{N} \Big[i\gamma\cdot D - M_N \\ & - \frac{g_A}{2f_\pi} (\gamma\cdot D \pi_a) \tau_a \gamma_5 + \frac{\kappa}{4M_N} \gamma^{\mu\nu} F_{\mu\nu} \Big] N \\ & - \frac{e^2}{32\pi^2 f_\pi} F_{\mu\nu} \tilde{F}^{\mu\nu} \pi_3 + \cdots, \end{aligned} \tag{8}$$

where π_a represents the isovector pseudoscalar pion field, N is the isodoublet spinor field of the nucleon, τ_a are the isospin Pauli matrices, $D_\mu = \partial_\mu - ieQA_\mu$ (with Q representing the electric charge isospin operator [$Q_\pi = -i\varepsilon^{ab3}$, $Q_N = \frac{1}{2}(1+\tau_3)$]), A_μ the electromagnetic field, $F_{\mu\nu} = \partial_\mu A_\nu - \partial_\nu A_\mu$, $\tilde{F}^{\mu\nu} = \frac{1}{2}\varepsilon^{\mu\nu\alpha\beta} F_{\alpha\beta}$, and κ is the anomalous magnetic moment of the nucleon ($\kappa_p \simeq 1.79$, $\kappa_n \simeq -1.91$).

Next we specify the terms involving the Δ field. Describing the Δ field by an isospin-3/2, spin-3/2 Rarita-Schwinger (RS) vector spinor $\Delta_\mu(x)$, we write the Δ piece of the chiral Lagrangian in the following form:

$$\mathcal{L} = \mathcal{L}_{RS} + \mathcal{L}_{\pi N\Delta} + \mathcal{L}_{\gamma N\Delta} + \cdots, \tag{9}$$

$$\mathcal{L}_{RS} = \overline{\Delta}_\mu (i\gamma^{\mu\nu\alpha}\partial_\alpha - M_\Delta \gamma^{\mu\nu}) \Delta_\nu, \tag{10}$$

$$\mathcal{L}_{\pi N\Delta} = \frac{ih_A}{2f_\pi M_\Delta} \overline{N} T_a^\dagger \gamma^{\mu\nu\lambda} (\partial_\mu \Delta_\nu) \partial_\lambda \pi^a + \text{H.c.}, \tag{11}$$

$$\begin{aligned}\mathcal{L}_{\gamma N\Delta} = {} & \frac{3e}{2M_N(M_N+M_\Delta)} \overline{N} T_3^\dagger (i g_M \tilde{F}^{\mu\nu} - g_E \gamma_5 F^{\mu\nu}) \partial_\mu \Delta_\nu \\ & + \text{H.c.} \end{aligned} \tag{12}$$

These are the free spin-3/2 Lagrangian, and the $\pi N\Delta$ and $\gamma N\Delta$ couplings, respectively. Here T_a are the isospin-1/2–isospin-3/2 transition matrices satisfying $T_a^\dagger T_b = \frac{2}{3}\delta_{ab} - \frac{1}{3} i\varepsilon_{abc}\tau_c$.

We have kept only the couplings that are linear in the Δ field and lowest order in the pion and the photon fields. In

[2]Our conventions: metric tensor $g^{\mu\nu} = \text{diag}(1,-1,-1,-1)$; γ-matrices γ^μ, $\gamma^5 = i\gamma^0\gamma^1\gamma^2\gamma^3$, $\{\gamma^\mu,\gamma^\nu\} = 2g^{\mu\nu}$; fully antisymmetrized products of γ matrices $\gamma^{\mu\nu} = \frac{1}{2}[\gamma^\mu,\gamma^\nu] = \gamma^\mu\gamma^\nu - g^{\mu\nu}$, $\gamma^{\mu\nu\alpha} = \frac{1}{2}\{\gamma^{\mu\nu},\gamma^\alpha\} = i\varepsilon^{\mu\nu\alpha\beta}\gamma_\beta\gamma_5$, $\gamma^{\mu\nu\alpha\beta} = \frac{1}{2}[\gamma^{\mu\nu\alpha},\gamma^\beta] = i\varepsilon^{\mu\nu\alpha\beta}\gamma_5$; spinor indices are omitted.

principle, there are many other couplings ($\pi\pi NN$, $\pi\pi N\Delta$, $\gamma\Delta\Delta$, etc.), represented in Eqs. (8) and (9) by the dots, which are required by the chiral and electromagnetic gauge symmetries. However, they are not relevant for our calculation at the order considered here.

For the purpose of power counting, we rearrange the interaction Lagrangian according to the number of small quantities (momentum, pion mass, and factors of e) that each term carries:

$$\mathcal{L}_I = \sum_i \mathcal{L}^{(i)},$$

$$\mathcal{L}^{(1)} = -\frac{g_A}{2f_\pi}\bar{N}(\gamma\cdot\partial\pi_a)\tau_a\gamma_5 N + \frac{ieQ_\pi g_A}{2f_\pi}\bar{N}\gamma\cdot A\pi\tau\gamma_5 N + e\bar{N}Q_N\gamma\cdot AN + \mathcal{L}_{\pi N\Delta},$$

$$\mathcal{L}^{(2)} = \frac{\kappa}{4M_N}\bar{N}\gamma^{\mu\nu}NF_{\mu\nu} + \tfrac{1}{2}(ieQ_\pi\pi A\cdot\partial\pi + \text{H.c.}) + e^2Q_\pi^2A^2\pi\pi + \mathcal{L}^{(g_M)}_{\gamma N\Delta}, \tag{13}$$

$$\mathcal{L}^{(3)} = \mathcal{L}^{(g_E)}_{\gamma N\Delta},$$

$$\mathcal{L}^{(4)} = -\frac{e^2}{32\pi^2 f_\pi}F_{\mu\nu}\tilde{F}^{\mu\nu}\pi_3.$$

A. Spin-3/2 gauge invariance

It is important to note that our $N\Delta$ couplings, besides being chiral and gauge invariant, are invariant under the following local (gauge) transformation of the spin-3/2 field:

$$\Delta_\mu(x) \to \Delta_\mu(x) + \partial_\mu\epsilon(x), \tag{14}$$

where ϵ is a spinor. This invariance ensures that the spin-3/2 field has the correct number of spin degrees of freedom (i.e., $2s+1=4$), cf. Refs. [27,28].

As a result of this additional symmetry, any vertex involving a Δ field, $\Gamma^\mu(p,\ldots)$, with μ being the vector index and p the 4-momentum of the Δ, will obey the *transversality condition*

$$p_\mu\Gamma^\mu(p,\ldots) = 0. \tag{15}$$

Using the well-known form of the spin-3/2 propagator,

$$S^{\mu\nu}(p) = \frac{1}{\not{p}-M_\Delta}\left[-g^{\mu\nu} + \frac{1}{3}\gamma^\mu\gamma^\nu + \frac{1}{3M_\Delta}(\gamma^\mu p^\nu - \gamma^\nu p^\mu) + \frac{2}{3M_\Delta^2}p^\mu p^\nu\right], \tag{16}$$

it is easy to show that the spin-1/2 sector of the RS propagator decouples [28], and one may equivalently use the following propagator:

$$\tilde{S}_{\mu\nu}(p) = \frac{-1}{\not{p}-M_\Delta}\mathcal{P}^{(3/2)}_{\mu\nu}(p), \tag{17}$$

where $\mathcal{P}^{(3/2)}_{\mu\nu}(p) = g_{\mu\nu} - \frac{1}{3}\gamma_\mu\gamma_\nu - (1/3p^2)(\not{p}\not{\gamma}_\mu p_\nu + p_\mu\gamma_\nu\not{p})$ is the spin-3/2 projection operator.

As a matter of fact, it is then also possible to replace the vertices as follows:

$$\tilde{\Gamma}_\mu(p,\ldots) = \mathcal{P}^{(3/2)}_{\mu\nu}\Gamma^\nu(p,\ldots). \tag{18}$$

In this theory, $\tilde{\Gamma}$ and Γ are completely equivalent. Nevertheless, vertices $\tilde{\Gamma}$ are sometimes more convenient in actual calculations. For example, the $\pi N\Delta$ vertex from Eq. (11):

$$\Gamma^\mu(p,k) = (g/M_\Delta)\gamma^{\mu\alpha\beta}p_\alpha k_\beta, \tag{19}$$

where $g \equiv h_A/2f_\pi$ and k is the pion four-momentum, can be replaced by

$$\tilde{\Gamma}_\mu(p,k) = (g/M_\Delta)\not{p}\mathcal{P}^{3/2}_{\mu\nu}(p)k^\nu, \tag{20}$$

where we have used $p^\mu\mathcal{P}^{3/2}_{\mu\nu}(p) = 0 = \gamma^\mu\mathcal{P}^{3/2}_{\mu\nu}(p)$. Furthermore, using $\mathcal{P}^{3/2}\mathcal{P}^{3/2} = \mathcal{P}^{3/2}$ and $[\not{p},\mathcal{P}^{3/2}(p)] = 0$, Δ-exchange amplitudes are computed effortlessly, e.g.,

$$\Gamma^\mu(p,k')S_{\mu\nu}(p)\Gamma^\mu(p,k) = \tilde{\Gamma}^\mu(p,k')\tilde{S}_{\mu\nu}(p)\tilde{\Gamma}^\mu(p,k) = \frac{-g^2}{\not{p}-M_\Delta}\frac{p^2}{M_\Delta^2}\mathcal{P}^{(3/2)}_{\mu\nu}(p)k'^\mu k^\nu. \tag{21}$$

B. Relation to conventional Δ couplings

Our $N\Delta$ couplings are rather different from the usual ones of, e.g., Refs. [13,19,22–24]. As a rule, standard couplings do not have the spin-3/2 gauge symmetry (14). Exceptions are the $\gamma N\Delta$ coupling of Jones and Scadron [30], which obviously satisfies Eq. (15), and the couplings used by Kondratyuk and Scholten [15]. We have adopted the Jones and Scadron convention for the magnetic ($M1$) coupling, g_M, in Eq. (12).

Other conventional couplings, including the G_1, G_2 representation of the $\gamma N\Delta$ vertex, do not have the spin-3/2 gauge symmetry. As a result, they involve the unphysical lower-spin sectors of the spin-3/2 field, and hence observables become dependent on arbitrary ''spin-1/2 backgrounds'' associated with off-shell parameters of the Δ. Other pathologies (see Ref. [27] and references therein)—all of which can be traced back to the fact that the couplings violate the degrees-of-freedom-counting constraints of the free theory—also occur in these theories.

One can establish a relation between the ''inconsistent'' and ''consistent'' couplings using field transformations [31], but this relation holds only in perturbation theory,[3] and so is

[3]Even then, it holds only if the ''naive'' Feynman rules apply in the inconsistent theory, which, strictly speaking, is not true [27].

not strictly applicable when resummation of the Δ contributions is necessary, as is the case in the computation shown in the following section.

III. COMPTON AMPLITUDE IN THE δ EXPANSION

In Compton scattering the momenta of the particles are characterized by the photon energy ω. For very low photon energies pions can be ''integrated out'' of the theory, with all nonanalytic effects associated with their production being replaced by a power series in ω/m_π (see, for instance, Ref. [32]). Clearly, the condition for this EFT to be effective is $\omega \ll m_\pi$. If, instead, we want to develop an EFT for $\omega \sim m_\pi$, we must treat both ω and m_π as low-energy scales, which means that pions must appear in the theory as explicit degrees of freedom.

Similarly, for the next relevant scale, $\Delta \equiv M_\Delta - M_N \approx 293$ MeV. A theory which does not treat it as a low-energy scale is effective only for $\omega \ll \Delta$. χPT without explicit Δs is an example of such an EFT. There only m_π is treated as a small scale, and it is assumed that $\omega \sim m_\pi \ll \Delta$. To extend this description to the Δ region, $\omega \sim \Delta$, we need to adopt Δ as a low-energy scale and include the Δ as an explicit degree of freedom. Thus, we naturally arrive at the scale hierarchy:

$$m_\pi \ll \Delta \ll \Lambda. \tag{22}$$

This hierarchy complies with the assumption of χPT, $m_\pi \ll \Delta$, and so χPT still gives the dominant effects in the theory if $\omega \sim m_\pi$. At the same time, Eq. (22) allows us to extend χPT to the Δ region.

In developing our power counting below, we will often keep the dependence of amplitudes on m_π and Δ explicit, so that the behavior of the amplitudes in the (independent) chiral ($m_\pi \to 0$) or the large-N_c ($\Delta \to 0$) limits is manifest [33]. Nevertheless, for the purposes of assigning an overall size to the amplitude arising from a particular graph or set of graphs, we would like to have one expansion parameter:

$$\delta \equiv \frac{\Delta}{\Lambda} \approx \frac{m_\pi}{\Delta}, \tag{23}$$

where we conservatively adopt $\Lambda \approx 600$ MeV, the scale introduced by the excitation energy of the next baryon resonance. In fact, Λ will represent not only this scale but all of the various high-energy scales, such as m_ρ, M_N, M_Δ, and $4\pi f_\pi$. Obviously, in this counting, Δ scales as δ, while m_π scales as δ^2.

While δ is of order one-half, the expansion in powers of δ is, in principle, no worse than χPT (which is an expansion in m_π/Δ) or the SSE [24] (which is an expansion in powers of Δ/Λ). Note that, since Eq. (23) is not necessarily true in worlds with other values of N_c, m_q, etc., once that equation is employed, the connection to the limits $m_q \to 0$ and $N_c \to \infty$ is lost unless the chiral and large-N_c limits are taken simultaneously with $m_\pi N_c^2$ held fixed.

We assign to each graph an overall δ-counting index α, which simply tells us that the graph is of size $e^2 \delta^\alpha / \Lambda$. Because we deal with two different low-energy scales in our EFT, the index α has two different expressions, depending on whether the photon energy ω is in the vicinity of m_π or Δ. For a graph with L loops, N_π pion propagators, N_N nucleon propagators, N_Δ Δ propagators, and V_i vertices of dimension i, the index is

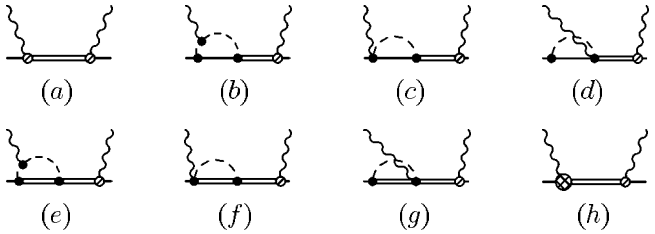

FIG. 1. Eight graphs which are one-Δ-reducible (OΔR), and so become enhanced in the region $\omega \sim \Delta$. The sliced vertex is the $M1$ $\gamma N\Delta$ vertex, while the sliced and diced $\gamma N\Delta$ vertex is the $E2$ coupling from $\mathcal{L}^{(3)}$. Solid dots represent couplings from $\mathcal{L}^{(1)}$.

$$\alpha = \begin{cases} 2\alpha_{\chi\mathrm{PT}} - N_\Delta, & \omega \sim m_\pi \\ \alpha_{\chi\mathrm{PT}} - N_\Delta, & \omega \sim \Delta, \end{cases} \tag{24}$$

where $\alpha_{\chi\mathrm{PT}} = \Sigma_i i V_i - 2 + 4L - N_N - 2N_\pi$ is the index of the graph in χPT without explicit Δs.

In deriving this power counting, we have used the fact that no graphs containing vertices with powers of m_π^2 or Δ occur up to the order to which we work. Such vertices do arise in higher-order graphs though. In general then, a vertex with j derivatives, k insertions of the quark mass, and l powers of the $\Delta - N$ mass difference scales as $\omega^j m_\pi^{2k} \Delta^l$, and so has overall dimension $i = j + 2k + l$. Denoting the number of such vertices by V_{jkl}, the δ index of an arbitrary graph is

$$\alpha = \begin{cases} \displaystyle\sum_{jkl} (2j + 4k + l) V_{jkl} + 2(4L - N_N - 2N_\pi - 2) - N_\Delta, \\ \qquad \omega \sim m_\pi; \\ \displaystyle\sum_{jkl} (j + 4k + l) V_{jkl} + 4L - 2 - N_N - 2N_\pi - N_\Delta, \\ \qquad \omega \sim \Delta, \end{cases}$$

which obviously reduces to Eq. (24) if only vertices with $k = l = 0$ are present.

In the region $\omega \sim \Delta$, there is an important exception to this scaling rule. Graphs that are one-Δ-reducible (OΔR), such as those in Fig. 1, scale not as δ^α but as

$$\delta^\alpha \left(\frac{1}{\omega - \Delta} \right)^{N_{O\Delta R}}, \tag{25}$$

where N_Δ in the equation for α now counts only the one-Δ-irreducible propagators, while $N_{O\Delta R}$ is the number of OΔR propagators. In the low-energy region this does not affect the power counting; however, in the region $\omega \sim \Delta$, these graphs can be dramatically enhanced. This forces us to resum all the OΔR contributions, which amounts to dressing the Δ propagator, thus ameliorating the divergence that oth-

TABLE I. The three different expansions discussed in the text. In all three cases the small expansion parameter is of order 1/2, and Λ is the breakdown scale of the theory.

Expansion	m_π/Λ	Δ/Λ
HBχPT	q	1
SSE	ϵ	ϵ
δ Expansion	δ^2	δ

erwise occurs at the Δ pole, and producing a width for the Δ of roughly the experimentally observed size.

Details of the dressing are given below. By definition, once dressing is performed, a OΔR graph can have only one Δ propagator, and such a graph then scales as

$$\delta^\alpha\left(\frac{1}{\omega-\Delta-\Sigma}\right), \tag{26}$$

where Σ is the self-energy. The expansion for Σ begins at δ^3, and so in the domain $|\omega-\Delta|\sim\delta^3$ the OΔR graphs are enhanced by δ^{-2} over the value expected from Eq. (24). Thus, the correct index of a OΔR graph in the region $\omega\sim\Delta$ is

$$\alpha=\alpha_{\chi\mathrm{PT}}-N_\Delta-2. \tag{27}$$

As a result, for instance, the *s*-channel-pole Δ graph of Fig. 1(a), which is the simplest OΔR graph, is promoted from NNLO in the low-energy region to LO in the Δ region.

The rest of this section is organized as follows. Before giving a detailed explanation of Compton counting in the δ expansion, we make a few comments on how our scheme compares to standard HBχPT and to the SSE of Refs. [23,24]. We then discuss power counting for the low-energy region $\omega\sim m_\pi$. In Sec. III C we explain the central issue for the higher-energy domain $\omega\sim\Delta$, the dressing of the Δ pole. Then in Sec. III D we elucidate the impact of this dressing on the counting for Compton-scattering graphs.

A. Comparison with HBχPT/SSE

In HBχPT the Δ is not included as an explicit ''low-energy'' degree of freedom in the Lagrangian. Instead, it is integrated out of the theory, producing a low-energy theory that, in principle, breaks down for $\omega\sim\Delta$. Power counting of graphs is then performed in terms of the index q, where

$$q\equiv\frac{\omega}{\Lambda}\sim\frac{m_\pi}{\Lambda}, \tag{28}$$

where Λ is usually assumed to be of order 1 GeV, although the omission of explicit Δs suggests instead $\Lambda\sim\Delta$.

Hemmert *et al.* [23,24] introduced the SSE (see also Ref. [29]), where the EFT expansion parameter is

$$\epsilon\equiv\frac{m_\pi}{\Lambda},\ \frac{\omega}{\Lambda},\ \frac{\Delta}{\Lambda}. \tag{29}$$

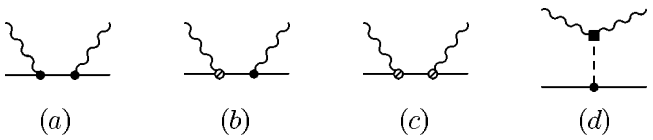

FIG. 2. The four relativistic tree-level graphs without Δs, which are included in our calculation. (We also include graphs generated from these graphs by crossing and/or time reversal.) The dot is the leading-order γNN coupling, while the sliced vertex is the anomalous-magnetic-moment vertex from $\mathcal{L}^{(2)}$. The square indicates the $\pi^0\to\gamma\gamma$ vertex from $\mathcal{L}^{(4)}$ which generates the chiral anomaly.

The SSE treats m_π and Δ as the same scale, and hence the Δ must be included explicitly in both energy domains, $\omega\sim m_\pi$ and $\omega\sim\Delta$.

This overemphasizes the importance of the Δ somewhat at low energies. In contrast, in the low-energy region, the δ-expansion amplitude is akin to that of HBχPT. In the region $\omega\sim\Delta$ the dressing of the Δ implemented here is not performed in either HBχPT—naturally, since Δs are ''high-energy'' degrees of freedom—or the SSE, as for $\omega\sim\Delta\sim m_\pi$ all πN loop effects are a small correction to the ''bare'' Δ propagator.

The table below (Table I) summarizes the relationship of the δ expansion to HBχPT and the SSE.

B. Power counting for $\omega\sim m_\pi$

Here we make the identification $\omega, m_\pi\sim\delta^2$. Graphs without Δ propagators then scale exactly as in χPT, but with small momenta $q\equiv\delta^2$.[4] The general index of such a graph is then given by Eq. (24). The leading contribution then comes from the sum of the relativistic nucleon Born graph (with $V_1=2,\ N_N=1,\ L=N_\pi=N_\Delta=0$) depicted in Fig. 2(a) and its crossed partner. Both graphs behave as $e^2/\omega\sim\delta^{-2}$ as $\omega\to0$. But the divergent parts cancel in the sum, as the low-energy theorem tells us they must [34]. The dominant term for small ω is given by the ''Thomson amplitude''

$$T^{(\mathrm{Th})}=-\frac{(\mathcal{Z}e)^2}{M_N}\boldsymbol{\varepsilon}'\cdot\boldsymbol{\varepsilon}, \tag{30}$$

with $\boldsymbol{\varepsilon}$ and $\boldsymbol{\varepsilon}'$ the photon's initial- and final-state polarization vectors. This, obviously, is $O(\delta^0)$.

When the expansion of the relativistic graphs [Figs. 2(a) and 2(b)] in powers of ω is made, there are also pieces $\sim e^2\omega=O(\delta^2)$. These form part of the NLO amplitude. The rest of the NLO amplitude is obtained from graphs which have index $\alpha=2$: nucleon tree graphs with the anomalous-magnetic-moment coupling (i.e., $V_2=2,\ N_N=1,\ L=N_\pi=N_\Delta=0$), see Fig. 2(c), and the π^0 exchange graph [Fig. 2(d)] involving the WZW anomaly, which has $V_1=V_4=1,\ N_\pi=1,\ L=N_N=N_\Delta=0$.

[4]The electron charge is usually counted as one power of q in χPT, and thus $O(q^3)=O(e^2q)$ for Compton scattering. Here we do not count the factor of e^2, which is present in all Compton graphs when assessing the δ index of a graph.

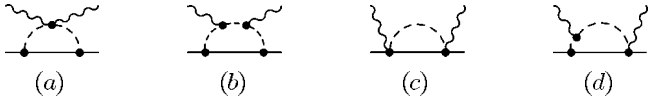

FIG. 3. The dominant πN-loop contributions to γN scattering (crossed and time-reversed partners are not shown, but are included).

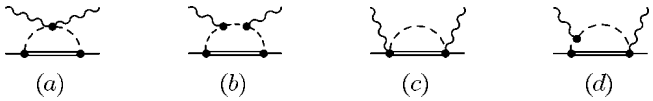

FIG. 4. The dominant $\pi\Delta$-loop contributions to γN scattering. Again, graphs generated from these by crossing and/or time reversal are not shown.

Next we consider πN-loop contributions to γN scattering. After making a heavy-baryon expansion of our relativistic Lagrangian, in order to avoid difficulties with the appearance of the scale M_N inside loops,[5] we construct the leading loop graphs from vertices in $\mathcal{L}^{(1)}$. This yields the graphs of Fig. 3, together with their crossed partners, as reviewed in Ref. [19]. These graphs are specified by $L=1$, $N_N=1$, $N_\Delta=0$, and either ($V_1=V_2=2$, $N_\pi=3$), ($V_1=2$, $N_\pi=1$), or ($V_1=2$, $V_2=1$, $N_\pi=2$); and hence all have $\alpha=2$. They are the only loop graphs with this counting index if we adopt Coulomb gauge and employ the heavy-baryon expansion. Explicit computation [17,19] reveals that the sum of these graphs indeed produces a Compton amplitude that behaves as

$$T^{(\pi N\ \mathrm{loop})}=\frac{e^2}{(4\pi f_\pi)^2}\frac{\omega^2}{m_\pi}F^{(1)}\left(\frac{\omega}{m_\pi}\right), \tag{31}$$

where $F^{(1)}$ is a nonanalytic function whose form is given in detail for the various possible spin and polarization structures in Refs. [17,19] and in Appendix A. $F^{(1)}$ has the property that $F^{(1)}\sim 1$ for $\omega\lesssim m_\pi$. A crucial feature of Eq. (31) is the fact that the sum of these leading loop graphs is proportional to ω^2. This is also a consequence of the low-energy theorem [34].

The counting formula (24) indicates that loop graphs with insertions from the second-order χPT Lagrangian $\mathcal{L}^{(2)}$ are down by two further powers of δ, being of $O(\delta^4)$. Relativistic corrections to Eq. (31) are suppressed by ω/M, and so are $O(\delta^4)$. Some loop graphs at $O(\delta^4)$ require renormalization, and the corresponding counterterms must be included. Meanwhile, graphs with two πN loops are $O(\delta^6)$ in this counting. Thus—at least in this energy domain—it is not until $O(\delta^6)$ that two-pion intermediate states contribute to the γN amplitude. And graphs involving additional πN rescatterings are similarly suppressed. Considering more loops and/or insertions with more derivatives only serves to further increase the δ index of graphs. Thus unitarity (in both the πN and $\pi\pi N$ channels) is violated in our calculation, but the violation is always an effect of an order beyond that at which we work.

Graphs containing the Δ begin to contribute at $O(\delta^3)$. The tree graph with two $M1$ $\gamma N\Delta$ vertices—see Fig. 1(a)—has $\alpha=3$ ($V_2=2$, $N_\Delta=1$, $L=N_N=N_\pi$). Meanwhile, the counting of the one-$\pi\Delta$-loop graphs, Fig. 4, is analogous to that for the πN loops, the only difference being that now $N_N=0$, $N_\Delta=1$ instead of $N_N=1$, $N_\Delta=0$. This results in the sum of the graphs in Fig. 4 being $O(\delta^3)$, i.e., scaling as

$$T^{(\Delta\pi\ \mathrm{loop})}=\frac{e^2}{(4\pi f_\pi)^2}\frac{\omega^2}{\Delta}H^{(1)}\left(\frac{\omega}{\Delta},\frac{m_\pi}{\Delta}\right), \tag{32}$$

where $H^{(1)}$ is a nonanalytic function which is of order one for $m_\pi/\Delta\sim\delta$, and $\omega/\Delta\lesssim 1$. Equation (32) is consistent with the low-energy theorem, and agrees with the explicit computation performed for these loops in Ref. [24].

In summary, in the δ expansion the Thomson term is the leading mechanism for Compton scattering on the nucleon at low energies, $\omega\sim m_\pi$. In this region pion loops are suppressed by one power of $\omega\sim m_\pi\sim\delta^2$, exactly as in HB$\chi$PT. If explicit Δs are included in the theory, the leading Δ-pole and $\Delta\pi$-loop graphs are suppressed by δ^3 relative to leading. They thus occur one order higher in the δ expansion than the $N\pi$ loop graphs of Fig. 3. They are, however, still one power of δ^{-1} larger than graphs arising from $\mathcal{L}^{(2)}$ insertions in πN loop graphs.

C. Dressing the Δ

The key issue for the theory in the region $\omega\sim\Delta$ is the treatment of the Δ pole. One-Δ-reducible (OΔR) graphs must be resummed in order to remove the divergence which otherwise occurs when $\not{p}=M_\Delta$.

Formally, all OΔR graphs can be summed via the series

$$S_{\mu\nu}(p)=S^{(0)}_{\mu\nu}(p)+S^{(0)}_{\mu\mu'}(p)\Sigma^{\mu'\nu'}(p)S^{(0)}_{\nu'\nu}(p)+\cdots, \tag{33}$$

where $\Sigma^{\mu\nu}(p)$ is the full one-Δ-irreducible (OΔI) Δ self-energy, and $S_{\mu\nu}(p)$ ($S^{(0)}_{\mu\nu}(p)$) is the dressed (bare) Δ propagator.

The function $\Sigma_{\mu\nu}$ has a δ expansion of its own,

$$\Sigma_{\mu\nu}=\Sigma^{(3)}_{\mu\nu}+\Sigma^{(4)}_{\mu\nu}+\cdots. \tag{34}$$

This expansion begins at $O(\delta^3)$, with the graphs depicted in Fig. 5, together with the counterterms necessary for their renormalization. Insertions from $\mathcal{L}^{(2)}_{\pi N}$ generate effects in $\Sigma^{(4)}$. These effects include relativistic corrections to the

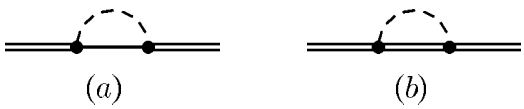

FIG. 5. πN and $\pi\Delta$ contributions to the Δ self-energy Σ. The vertices are from $\mathcal{L}^{(1)}$ and so both graphs are $O(\delta^3)$.

[5]The ideal solution to this difficulty would be to use infrared regularization [35] to compute the πN loops. But the result of such a computation should only differ from the HBχPT one by terms suppressed by δ. Such terms are of higher order than considered here.

leading heavy-baryon result $\Sigma^{(3)}$. Two-loop contributions to the self-energy—including the leading effect of the $N\pi\pi$ channel—first occur in $\Sigma^{(5)}$, and are thus smaller by δ^2 than the dominant piece of Σ.

If

$$|\omega-\Delta|\sim\delta^3 \tag{35}$$

and we keep only the third-order piece of the self-energy, then all terms on the right-hand side of Eq. (33) are of the same order. A perturbative expansion of the right-hand side—which is certainly valid for $|\omega-\Delta|\sim\delta^2$ or larger—is no longer appropriate. Instead, if Eq. (35) holds, the whole series must be resummed, giving

$$S_{\mu\nu}(p)=\frac{-1}{\not p-M_\Delta-\overline{\Sigma}^{(3)}(p)}\mathcal{P}^{(3/2)}_{\mu\nu}(p). \tag{36}$$

Equation (35) then defines precisely what we mean by $\omega\sim\Delta$.

In fact, the most general Lorentz-covariant form of $\Sigma^{\mu\nu}(p)$ is rather complicated. It contains up to ten independent scalar functions. As a result, the dressed propagator does not generally have the form (36). This is a consequence of using ''inconsistent'' spin-3/2 couplings—ones that *do not* obey the symmetry under Eq. (14). If, however, couplings which are consistent in that sense are used, then the Δ self-energy can be written as

$$\Sigma^{\mu\nu}(p)=\Sigma(p)\mathcal{P}^{(3/2)\mu\nu}(p), \tag{37}$$

with $\Sigma(p)$ akin to the usual fermion self-energy, $\Sigma(p)=A(p^2)\not p+B(p^2)$, where A and B are scalar functions. Dressing then affects only the spin-3/2 piece of the propagator and the results of form (36). The divergence at $\not p=M_\Delta$ is ameliorated, and no further resummation is necessary. δ Counting indicates that the effects of $\Sigma^{(n)}$ for $n\geq 4$ can be included by perturbing around propagator (36).

Δ Propagators of this form have been used in other authors' extensions of chiral perturbation theory to the resonance region [36–38], although in these works it is not clear why only the spin-3/2 sector is dressed. Note that in contrast to the work of, for instance, Ref. [37], we do not dress the nucleon pole by πN loops. Arguments analogous to those of this section suggest that nucleon dressing is only necessary from a power-counting point of view for $\omega\sim 0$, and there $\Sigma(p)$ is purely real. As we shall now see, after renormalization the real part of $\Sigma^{(3)}$ plays a negligible role in propagator (36).

In Eq. (36) the quantity $\overline{\Sigma}^{(3)}$ indicates that we are resumming the renormalized third-order Δ self-energy. The explicit renormalization of this quantity will be performed elsewhere. Here we make a more general argument which constrains the form and importance of any renormalized self-energy appearing in Eq. (36).

First, observe that the general Lorentz structure of the self-energy Σ results in

$$S_{\mu\nu}(p)=-\frac{Z(p^2)}{\not p-M(p^2)}\mathcal{P}^{(3/2)}_{\mu\nu}(p), \tag{38}$$

with Z and M scalar functions of p^2. After mass, wave function, and coupling constant renormalization, these can be written as

$$Z(p^2)=1+(p^2-M_\Delta^2)f_Z(p^2)+i\,\mathrm{Im}Z(p^2), \tag{39}$$

$$M(p^2)=M_\Delta+(p^2-M_\Delta^2)^2 f_M(p^2)+i\,\mathrm{Im}M(p^2), \tag{40}$$

with f_Z and f_M real functions of p^2.

Substituting these forms into Eq. (38) we find that

$$S_{\mu\nu}(p)=-\frac{1+i\,\mathrm{Im}Z(p^2)}{\not p-M_\Delta-i\,\mathrm{Im}M(p^2)}\mathcal{P}^{(3/2)}_{\mu\nu}(p)+O\left(\frac{1}{\Lambda}\right). \tag{41}$$

In region (35), the pole piece is $O(\delta^{-3})$, while the remaining ''background'' terms are $O(\delta^0)$. Thus any corrections to $S_{\mu\nu}(p^2)$ from $\mathrm{Re}Z(p^2)$ or $\mathrm{Re}M(p^2)$ are three powers of δ beyond the leading one. Corrections from $\mathrm{Im}Z(p^2)$ are equally suppressed, since it too is $O(\delta^3)$.

Thus, up to corrections which are NNNLO, it is sufficient to compute only $\mathrm{Im}\,M(p^2)$. Provided that $\omega\leqslant\Delta+m_\pi$, this comes exclusively from Fig. 5(a). A straightforward calculation gives

$$\mathrm{Im}M(s)\equiv-\frac{\Gamma(s)}{2}=-\left(\frac{h_A}{2f_\pi}\right)^2\frac{s+M_N^2-m_\pi^2}{24\pi M_\Delta^2}k^3\theta(k), \tag{42}$$

where k is the on-shell value of the pion three-momentum,

$$k=\{[s-(M_N+m_\pi)^2][s-(M_N-m_\pi)^2]/(4s)\}^{1/2}\sim\delta. \tag{43}$$

Thus, the width is $O(\delta^3)$, as promised.

The final form of the resummed Δ propagator is then

$$S_{\mu\nu}(p)=-\frac{1}{\not p-M_\Delta+\frac{i}{2}\Gamma(p^2)}\mathcal{P}^{(3/2)}_{\mu\nu}(p). \tag{44}$$

If this propagator appears in a OΔR γN graph and Eq. (35) is satisfied, then it scales as δ^{-3}.

D. Power counting for $\omega\sim\Delta$

The effect of this modified scaling for the Δ propagator is that (dressed) OΔR graphs become the dominant effects for $\omega\sim\Delta$. Their δ index is given by Eq. (27). The Δ-pole graph in Fig. 1(a), with $M1$ $\gamma N\Delta$ vertices (i.e., $V_2=2$, $N_\Delta=1$), has $\alpha=-1$ in region (35) and gives the leading contribution there. The graph of Fig. 1(h) with one $E2$ coupling (i.e., $V_2=1$, $V_3=1$) has $\alpha=0$, and hence is of NLO if $\omega\sim\Delta$.

Meanwhile, the OΔR graphs of Figs. 1(b)–1(g) (and their time-reversed partners) are characterized by $L=N_N=N_\Delta=1$ and either $V_1=V_2=N_\pi=2$ or $V_2=N_\pi=1$, $V_1=2$.

They too have $\alpha=0$ and contribute at NLO. These loop graphs are divergent and must be renormalized. This is achieved via Fig. 1(h). The loop effects may then be included in the calculation by the use of an energy-dependent $E2$ coupling: $g_E \to g_E(s)$. The leading effect here again arises from the imaginary part of the loops, hence

$$g_E(s) = g_E + i\left(\frac{g_A h_A}{4f_\pi^2}\right)\frac{s+M_N^2-m_\pi^2}{24\pi s} \times \frac{M_N k^2}{\omega_\gamma}\,\frac{2M_N(M_N+M_\Delta)}{3M_\Delta \omega_\gamma} \times [Q_0(\omega_k/k) - Q_2(\omega_k/k)]\,\theta(k), \tag{45}$$

where $\omega_\gamma = (s-M_N^2)/2\sqrt{s}$, $\omega_k = \sqrt{m_\pi^2+k^2}$, while k is given by Eq. (43), and Q_l is the lth Legendre function of the second kind.

NLO effects can also be obtained by considering corrections from $\Sigma^{(4)}$ to the leading Δ self-energy $\Sigma^{(3)}$. More complicated electromagnetic couplings and higher-order terms in Σ lead to effects of NNLO in the δ expansion of OΔR graphs.

What is the δ index of graphs without a Δ pole? OΔI graphs such as $\Delta\pi$ and $N\pi$ loops obey Eq. (24)—they are not enhanced. They retain a positive δ index, and so are at least NNLO in this counting.

One might wonder how to reconcile this with Eq. (31) that seems to suggest that the δ scaling of the dominant πN loops will be, for $\omega \sim \Delta$,

$$e^2\frac{\omega^2}{m_\pi} = e^2\frac{\Delta^2}{\Delta^2} = e^2\delta^0. \tag{46}$$

This conclusion is erroneous because $F^{(1)}$ is not $O(1)$ if ω/m_π is large. If $\omega/m_\pi \gg 1$, the loop functions should be expanded about the large-ω limit, not the small ω one, and doing so results in

$$T^{(\pi N\ \text{loop})} = \frac{e^2}{(4\pi^2 f_\pi)^2}\left[c_1\omega + d_1 m_\pi + c_3\frac{m_\pi^2}{\omega} + c_5\frac{m_\pi^4}{\omega^3} + \cdots\right]. \tag{47}$$

Assigning $\omega \sim \Delta$, $m_\pi \sim \Delta^2$ we see that this series, rather than one in increasing powers of ω is the correct one for the ''medium-energy'' regime $\omega \sim \Delta \gg m_\pi$. This is completely opposite to a polarizability expansion in increasing powers of ω. In our approach $\omega \sim \Delta$ is sufficiently far from threshold, so that a power-series expansion around $\omega=0$ of Δ contributions is not very useful.

IV. IN PRACTICE

A. Defining the NLO calculation

To perform a complete NLO calculation in the whole energy region $0 < \omega \lesssim \Delta$, we include all of the nucleon pole and πN loop graphs of Figs. 2 and 3, together with their crossed partners. To these we add the OΔR graphs of Fig. 1, which in the low-energy region contribute at NNLO and above, but for $|\omega-\Delta| \sim \delta^3$ give effects of leading and next-to-leading order. We also include the OΔR graph with two g_E $\gamma N\Delta$ couplings, even though it is formally NNLO.

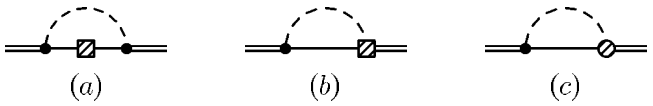

FIG. 6. Heavy-baryon expansion graphs that represent $O(\epsilon^4)$ πN-loop contributions to the Δ self-energy Σ. The sliced squares are vertices from the second-order $\pi N\Delta$ HB Lagrangian whose coefficient is fixed by Lorentz invariance. The sliced circle represents a vertex from $\mathcal{L}_{\pi N\Delta}$ with a coefficient which is *a priori* undetermined (see Ref. [40]).

We keep all of these effects in both kinematic regions. Note that this means we are always keeping contributions that are, strictly speaking, beyond the order to which we work. This is done in order to provide a smooth transition between the two different photon-energy domains. For the same reason, in both regions we always use the resummed Δ propagator (44).

The power counting of Sec. III C indicates that at NLO we must include effects due to the $O(\delta^4)$ piece of Σ, $\Sigma^{(4)}$. The heavy-baryon graphs which contribute to the $O(\epsilon^4)$ self-energy in a heavy-baryon calculation with explicit Δs [40] are shown in Fig. 6. The relativistic calculation of the Δ width, which led to Eq. (42), already includes the effects of Figs. 6(a) and 6(b). As for Fig. 6(c), this graph gives a contribution to Σ which behaves as [40]

$$\Sigma^{6(c)}(p) \sim \frac{(b_3+b_8)h_A}{f_\pi^2}\int \frac{d^4k}{(2\pi)^4}\,\frac{k^2}{k^2-m_\pi^2}\,\frac{v\cdot k}{v\cdot(p-k)}. \tag{48}$$

The imaginary part of this graph is proportional to $\omega k m_\pi^2$ [with k given by Eq. (43)], so while it is $O(\epsilon^4)$ in the SSE, in our counting it is $O(\delta^6)$, and so well beyond the order to which we work. Thus the result (42) is already accurate up to corrections of relative order δ^2.

The u-channel Δ-pole graph is NNLO throughout this entire energy region and is *not* included in our Compton amplitude. Therefore, by looking at its effect on cross sections, we can estimate the importance of NNLO contributions.

B. Covariant decomposition of the Compton amplitude

To compute the amplitude of Compton scattering on a spin-1/2 target in a manifestly Lorentz- and gauge-invariant form, we specify it in terms of eight scalar amplitudes $A_1, \ldots, A_8$ (instead of the usual six):

$$M_{fi} = e^2\bar{u}(p')\sum_{i=1}^{8} A_i(s,t)O_i^{\mu\nu}\mathcal{E}'^*_\mu(q')\mathcal{E}_\nu(q)u(p), \tag{49}$$

where p', p (and q', q) are the final and initial 4-momenta of the nucleon (and photon), respectively; u is the free nucleon spinor, $\mathcal{E}_\mu$ is a modified photon polarization vector:

$$\mathcal{E}_\mu(q)=\varepsilon_\mu-\frac{P\cdot\varepsilon}{P\cdot q}q_\mu, \tag{50}$$

with $P=p+p'$. Tensors O_i are given by

$$\begin{aligned}
O_1^{\mu\nu}&=-g^{\mu\nu},\\
O_2^{\mu\nu}&=q^\mu q'^\nu,\\
O_3^{\mu\nu}&=-\gamma^{\mu\nu},\\
O_4^{\mu\nu}&=g^{\mu\nu}(q'\cdot\gamma\cdot q),\\
O_5^{\mu\nu}&=q^\mu q'_\alpha\gamma^{\alpha\nu}-\gamma^{\mu\alpha}q_\alpha q'^\nu,\\
O_6^{\mu\nu}&=q^\mu q'_\alpha\gamma^{\alpha\nu}-\gamma^{\mu\alpha}q_\alpha q'^\nu,\\
O_7^{\mu\nu}&=q^\mu q'^\nu(q'\cdot\gamma\cdot q),\\
O_8^{\mu\nu}&=i\gamma_5\epsilon^{\mu\nu\alpha\beta}q'_\alpha q_\beta.
\end{aligned} \tag{51}$$

Mandelstam variables s, t, and u are defined as usual:

$$\begin{aligned}
s&=(p+q)^2=M_N^2+2p\cdot q,\\
t&=(q'-q)^2=-2q\cdot q',\\
u&=(p-q')^2=M_N^2-2p\cdot q',
\end{aligned} \tag{52}$$

where we have used the on-shell conditions $q^2=q'^2=0$ and $p^2=p'^2=M_N^2$. Note that $P\cdot q=\frac{1}{2}(s-u)=P\cdot q'$.

The representation (49) is obtained by writing down the most general covariant structure (for the on-shell situation) and imposing the electromagnetic current-conservation condition. Thus this representation incorporates both covariance and gauge invariance in a manifest way.

The amplitudes A_i are most easily computed in the following Lorentz-invariant gauge:

$$P\cdot\varepsilon=0=P\cdot\varepsilon'. \tag{53}$$

This condition can also be achieved in the Coulomb gauge ($\varepsilon_0=0=\varepsilon'_0$) by going to the Breit frame, $\vec{P}=0$.

In the Coulomb gauge, the structures O_1–O_6 exactly match the ones in the standard decomposition (e.g., Refs. [19,34]), while O_7 and O_8 can be reduced to linear combinations of O_3, O_5, and O_6,

$$O_7=(\omega^2+\tfrac{1}{2}t)[-tO_3+O_5]-\omega^2O_6, \tag{54}$$

$$O_8=\tfrac{1}{2}\omega(-tO_3+O_5-O_6). \tag{55}$$

In particular, the results for the nucleon-exchange (Born) graphs, the anomaly graph, and the Δ exchange graphs are specified in terms of the amplitudes $A_1,\ldots,A_8$ in Appendix A. As our calculation of these graphs is fully relativistic, it differs from that of HBχPT in Refs. [19,23] by terms of $O(\delta)$.

Meanwhile, for the πN loop graphs depicted in Fig. 3, we have used the $O(q^3)$ HBχPT result of Refs. [17,19]. This is done in order to avoid difficulties with the treatment of the nucleon mass scale M_N inside the loops. The amplitude obtained in a fully relativistic calculation of these loops would differ from the result used here by terms of $O(\omega/M)$ and $O(m_\pi/M)$, i.e., terms down by δ^2. The loop contributions are given in Appendix A.

We do include one particular relativistic effect because we write the photon energy ω that appears in the loop functions as $\omega=\sqrt{s}-M_N$. The standard choices for ω—center-of-mass photon energy [19] and Breit-frame photon energy [17]—differ from this by terms which are of N^{3}LO in our counting. We adopt this prescription in order to ensure that the Compton amplitude's πN cut occurs at the correct value of s.

V. RESULTS AND DISCUSSION

A. Differential cross sections for γp scattering

There are no γN contact terms at NLO in the δ expansion. This leaves us with three EFT parameters which must be fixed using the data: g_E, g_M, and h_A. For h_A we adopt the phenomenological value $h_A=2.81$ ($f^2_{\pi N\Delta}/4\pi\simeq 0.35$), which corresponds to a Δ width $\Gamma(M_\Delta^2)\simeq 111$MeV—consistent with the range given by the Particle Data Group [39]. This value of h_A is roughly 5% larger than that obtained from the large-N_c relation $h_A=(3/\sqrt{2})g_A$.

This leaves us with two free parameters, g_M and g_E, of the $\gamma N\Delta$ coupling (12). They represent the strength of, respectively, the $M1$ and $E2$ $\gamma N\to\Delta$ transitions.

In principle, these are relatively well known from pion photoproduction. In particular, their ratio is related to the $R_{EM}=E2/M1$ ratio,

$$R_{EM}=\frac{g_E\Delta}{2g_M(M_N+M_\Delta)-g_E\Delta}\times 100\%. \tag{56}$$

The determination of this ratio has recently been the subject of experimental programs at the JLab and the MAMI. The present Particle Data Group (PDG) value is $R_{EM}=(-2.5\pm 1.0)\%$ [39]. However, this number is measured only indirectly through the extraction of the ratio of the pion-photoproduction multipoles at the Δ-resonance position. These multipoles are affected by a number of background processes, and relationship (56) is only strictly true at leading order in the δ expansion for the $\gamma p\to\pi p$ amplitude. To fully understand the constraint that pion photoproduction places on g_E/g_M in this EFT, a higher-order calculation of $\gamma p\to\pi p$ using the δ expansion is necessary. (For an attempt to compute this process in the SSE, see Ref. [41].) Such a calculation being absent, here we regard g_M and g_E as free parameters and fit them to get the best agreement with γp cross-section data. An important future test of the usefulness of δ expansion will be whether the resultant value for g_E/g_M is ultimately consistent with that found from pion-photoproduction data using the same framework.

The results for the differential cross section at several different energies are presented in Figs. 7 and 8. The long-dashed orange curve represents a calculation which includes only the Born graphs of Fig. 2. The dashed blue curve is the

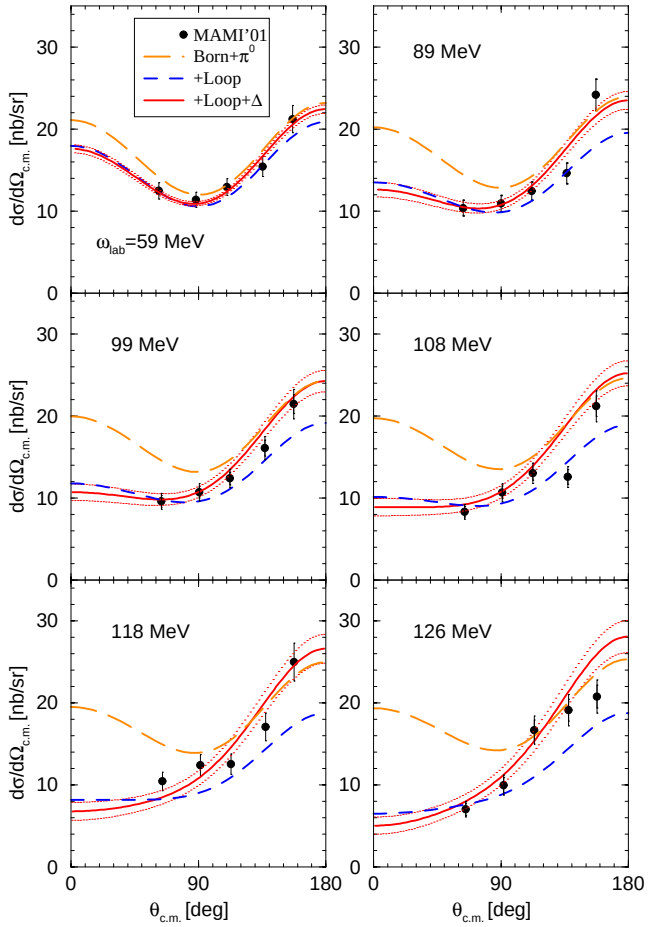

FIG. 7. Angular distribution of the γp differential cross section at low energies. Data points are from Ref. [5]. The long-dashed orange line represents the sum of nucleon and pion Born graphs, the blue dashed line gives the NLO χPT prediction, and the red solid line is the full result at NLO in the δ expansion. The dots give an estimate of the theoretical error.

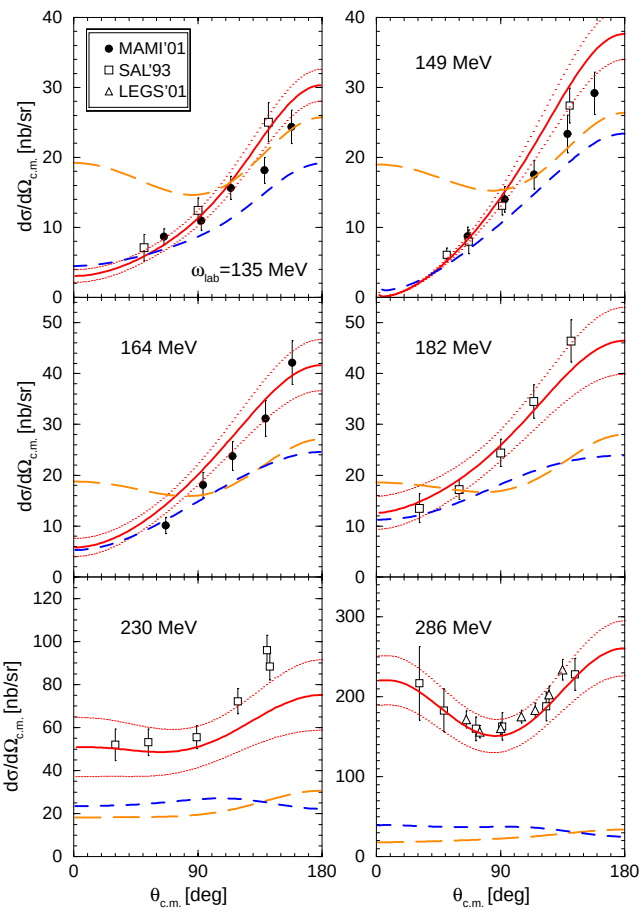

FIG. 8. Angular distribution of the γp differential cross section. Caption for the curves is the same as in Fig. 7. Data points are from Ref. [5] (MAMI'01), Ref. [1] (SAL'93), and Ref. [4] (LEGS'01).

result when the πN loops of Fig. 3 are added, and so gives the $O(q^3)$ prediction of HBχPT. Finally, the complete NLO calculation in the δ-expansion is represented by the solid red curve. The sharp rise at backward angles as ω increases past the pion-production threshold is now reproduced in the theory. This sharp rise is very difficult to obtain in χPT without explicit Δs.

In Figs. 7 and 8 we also show a theoretical error band, demarcated by the red dots. This is obtained by estimating the size of the NNLO contribution in the following way:

$$T(\text{theoretical error}) = -\frac{e^2}{M_N}\varepsilon'\cdot\varepsilon\times\begin{cases}\omega^2/\Delta, & \omega\sim m_\pi\\ \omega, & \omega\sim\Delta.\end{cases} \tag{57}$$

The error band in Figs. 7 and 8 is plotted with the border between the two kinematic domains at $\omega=200$ MeV. The band is an estimate of how far we expect the NNLO corrections to change the results. It may overestimate the theoretical error since our calculation already includes a number of NNLO contributions: relativistic effects coming from tree graphs, Δ-exchange (which is NNLO for $\omega\sim m_\pi$), and πN loops (which are NNLO for $\omega\sim\Delta$).

The fit of the cross section favors the following values for the $\gamma N\to\Delta$ parameters:

$$g_M = 2.6\pm 0.2, \quad g_E = -6.0\pm 0.9. \tag{58}$$

The solid line in Figs. 7 and 8 gives the result for the central values of g_M and g_E. The uncertainty in Eq. (58) is found by varying these couplings until the experimental cross section in the Δ region is no longer within the theoretical error band.

The resulting value of g_M is consistent with the large N_c value, $g_M=(2\sqrt{2}/3)(1+\kappa_p)\simeq 2.63$, while the value of g_E is considerably different from phenomenological expectations. For instance, from $R_{EM}=-2.5\%$ and Eq. (56), one would expect $g_E=-1$. This problem signifies the importance of performing an analogous calculation of pion photoproduction to check the consistency of the δ expansion.

Next we would like to note that, although formally the imaginary and real parts of $g_E(s)$ of Eq. (45) are of the same order, numerically the imaginary part is smaller by at least a factor of 6. Im$g_E(s)$ has a negligible impact on the angular distributions shown in Figs. 7 and 8.

The NLO prediction for the differential cross-section energy dependence is shown in Fig. 9 for a scattering angle of

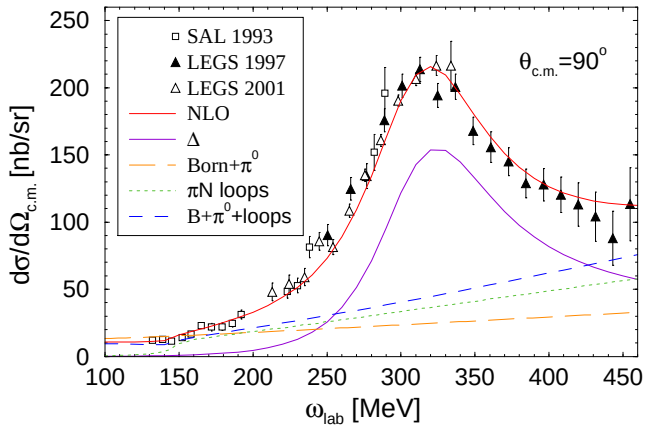

FIG. 9. Energy dependence of the γp differential cross section at 90°. Data points are from Ref. [1] (SAL'93), Ref. [3] (LEGS'97), and Ref. [4] (LEGS'01). The red solid, orange long-dashed, and blue dashed lines are as above, while the purple curve now gives the contribution arising solely from the Δ, and the green short-dashed curve is the effect of πN loops alone.

90°. The solid purple line is the result when only Δ-pole mechanisms are included, and g_M and g_E are chosen according to Eq. (58). The solid red line gives the result of our NLO calculation. Individual contributions from Born graphs and πN loops are given by the orange dashed and green short-dashed lines, respectively. The $O(q^3)$ prediction of HBχPT is represented by the blue dashed line. This figure shows that our NLO calculation of the Δ width is in good agreement with the data. This lends support to our adoption of the value $h_A=2.81$. However, it must be pointed out that since our EFT was only designed for $0\leqslant\omega\lesssim\Delta$, the agreement at the higher energies (which is seen in Fig. 9) is probably somewhat fortuitous.

B. Polarizabilities

The results for the nucleon polarizabilities are worked out in Appendix B. The leading contribution to polarizabilities is from πN loops and hence is exactly the same as in HBχPT, see Eq. (1). On the other hand, our results for the Δ contributions differ from earlier ones in several ways as follows.

(1) First of all, in contrast to the results of Refs. [13,22], they are independent of "off-shell parameters."

(2) The leading SSE result of Ref. [23] for the magnetic polarizability is also free of off-shell parameters (in the SSE they enter at NLO). Formally, the result of Appendix B agrees with that found in Ref. [23]—apart from a higher-order relativistic effect which is numerically only of order 10%:

$$\beta_N^{(\Delta)\ \text{this work}}=\frac{2}{2+\Delta}\beta_N^{(\Delta)\ \text{SSE}}.$$

However, our fit to the cross section prefers a significantly smaller value of the $\gamma N\Delta$ coupling than was used in Ref. [23], and this leads to a markedly smaller numerical result for $\beta_p^{(\Delta)}$.

TABLE II. Proton polarizabilities in χPT, the δ expansion, and the SSE, compared to values extracted from experiment. Results are in units of 10^{-4} fm^3.

Reference	α_p	β_p
NLO HBχPT [19]	12.2	1.2
NLO δ [this work]	$10.2^{+4.2}_{-2.0}$	$3.9^{+2.7}_{-0.4}$
NLO SSE [25] ([23])	16.4 (20.8)	9.1 (14.7)
PDG average [39]	12.0 ± 0.7	1.6 ± 0.6
LEGS [4]	11.8 ± 2.0	1.4 ± 1.5
MAMI [5]	11.9 ± 2.1	1.2 ± 1.4
Beane *et al.* [20]	12.1 ± 1.6	3.2 ± 1.2

(3) Perhaps most importantly, our NLO calculation includes neither u-channel Δ exchange nor $\pi\Delta$ loops, since both are NNLO in the δ expansion. In fact, the Δ contributions quoted in Appendix B stem from both the s- and u-channel Δ exchange graphs. However, the NLO calculation presented above has no u-channel graph. Thus to find the polarizabilities that correspond to the cross-section calculation of Sec. V A, one must halve the Δ pieces of polarizabilities given in Appendix B.

All of these effects produce a Δ contribution to the magnetic polarizability, which is significantly smaller than that found in previous EFT calculations with explicit Δ*s* [21–23,25]:

$$\beta_p^{(\Delta)}=\frac{\alpha g_M^2}{(M_N+M_\Delta)^2\Delta}=(2.7\pm0.4)\times10^{-4}\ \text{fm}^3. \quad (59)$$

The Δ contribution to the electric polarizability comes solely from the s-channel Δ pole with two g_E couplings:

$$\alpha_p^{(\Delta)}=-\frac{\alpha g_E^2}{(M_N+M_\Delta)^3}=(-2.0\pm0.7)\times10^{-4}\ \text{fm}^3. \quad (60)$$

The observant reader might have noticed that the inclusion of Δ contributions in the polarizabilities is not, strictly speaking, consistent at NLO in our power counting. The s-channel Δ pole is, like its u-channel counterpart, NNLO for $\omega\sim0$. In spite of this we have included the Δ contributions in the results shown in Table II. The numbers there represent the polarizabilities corresponding to the cross-section calculation already presented.

We expect that in an NNLO δ-expansion calculation the Δ's effect on β_p will roughly double. α_p will also be modified, thanks to the graphs in Fig. 4 and the u-channel Δ-pole graph with two g_E couplings. Estimating these effects gives the theory error bars that appear in the second line of the table. We note that, even though NNLO effects make a significant difference in the values for α_p and β_p, their impact on the low-energy differential cross section is not large, being represented by the theoretical error band in Fig. 7. This suggests that the extraction of polarizabilities from Compton data is a delicate process.

VI. CONCLUDING REMARKS

The expansion developed in this paper for the γN amplitude is based on the scale hierarchy $m_\pi \ll \Delta \ll \Lambda$. The EFT expansion parameter employed here is δ, which represents both the ratio of m_π to Δ and the ratio of Δ to Λ. The success of the resulting "δ expansion" is to be judged by its efficacy as an EFT of Compton scattering.

The existence of two different low-energy scales in the theory forces us to develop independent power countings for the two different photon-energy regimes. For $\omega \sim m_\pi$, the Compton amplitude obtained is exactly that of χPT up to effects from the Δ, which are down by δ^3 relative to leading. On the other hand, if $\omega \sim \Delta$, OΔR graphs dominate the Compton amplitude. Resummation of the Δ self-energy is necessary in these graphs. The Δ propagator appearing in them acquires a finite, energy-dependent width. Up to effects suppressed by δ^3, this is the only correction necessary to the Δ propagator. Vertex corrections also appear at NLO in this region.

We performed a calculation of the γN amplitude, which includes all effects that are of leading or next-to-leading order in the region $\omega \sim m_\pi$, as well as all effects that are of leading or next-to-leading order in the region $\omega \sim \Delta$. The sum of all of these pieces of the amplitude defines our NLO calculation. Thus, in each of the two regions considered, mechanisms of NNLO in that particular region are included in the calculation. Nevertheless, effects of relative order δ^3 (e.g., $\Delta\pi$ loops) are omitted in the low-energy region, while effects of relative order δ^2 (e.g., two-loop dressing of the Δ) are omitted in the higher-energy domain. These neglected effects define the theoretical error bar of our calculation.

Note that in this calculation tree-level graphs are computed relativistically, while for loop graphs we use the HBχPT result. While this gives the correct γN amplitude up to the order to which we work, a fully relativistic treatment of πN loops would be more aesthetically pleasing.

After fitting the only two free parameters in our theory, the $E2$ and $M1$ $\gamma N\Delta$ couplings, good agreement with the low-energy γp data is found. The spin-independent polarizabilities α and β that result from our NLO calculation are in reasonable agreement with contemporary extractions from data [5,20].

The development of the δ expansion opens up a number of avenues for further study. Higher-order calculations of Compton scattering on the nucleon will be necessary to see if the good agreement found at NLO persists, and if the expansion in powers of δ is well behaved or not. Also, the use of the δ expansion in other processes, e.g., pion photoproduction, is an important potential future application. Indeed, the EFT presented here should ultimately be judged by its success in simultaneously describing data on nucleon Compton scattering, pion photoproduction, and πN scattering. Only then can the reliability of the EFT, and hence of our extraction of g_E and g_M from γN data to NLO in the δ expansion, really be judged.

The use of the δ expansion in two-nucleon systems might also reap significant rewards. We plan to use the amplitude developed here, together with consistent two-body currents, in a calculation of γD scattering [42]. It is also possible that the δ expansion could be profitably employed to organize the Δ contributions to the chiral nucleon-nucleon potential developed in Refs. [43–45].

ACKNOWLEDGMENTS

We thank Sergey Kondratyuk and Olaf Scholten for comments on the manuscript. D. R. P. thanks Harald Grießhammer and Thomas Hemmert for useful discussions and the Benasque Centre for Science for its hospitality during part of this work. This research was supported by the U.S. Department of Energy under Grant Nos. DE-FG02-93ER40756, DE-FG02-02ER41218, and by the National Science Foundation under Grant No. NSF-SGER-0094668.

APPENDIX A: RESULTS FOR COMPTON INVARIANT AMPLITUDES

We define the photon energy as $\omega = (p\cdot q)/M_N = (s - M_N^2)/2M_N$. The results for the invariant amplitudes are presented in the nucleon mass units ($M_N = 1$). Below $\mathcal{Z} = 1$ for the proton, $\mathcal{Z} = 0$ for the neutron. Expressions for the Δ exchange are obtained using the algebraic manipulation program Form [46].

1. Nucleon s channel

$$A_1(\omega,t) = -\frac{1}{2}\left[\mathcal{Z}^2 + \frac{1}{4\omega}(\mathcal{Z}+\kappa)^2 t + \frac{1}{2}\kappa^2\left(\omega + \frac{1}{4}t\right)\right],$$

$$A_2(\omega,t) = \frac{\kappa}{2\omega}\left[\mathcal{Z} + \frac{1}{2}\kappa\left(1 - \frac{1}{2}\omega - \frac{1}{8}t\right)\right],$$

$$A_3(\omega,t) = A_1(\omega,t),$$

$$A_4(\omega,t) = -\frac{1}{4\omega}\left[(\mathcal{Z}+\kappa)^2 + \frac{1}{2}\kappa^2\omega\right],$$

$$A_5(\omega,t) = \frac{(\mathcal{Z}+\kappa)^2}{4\omega}, \tag{A1}$$

$$A_6(\omega,t) = -\frac{\mathcal{Z}(\mathcal{Z}+\kappa)}{4\omega},$$

$$A_7(\omega,t) = \frac{\kappa^2}{16\omega},$$

$$A_8(\omega,t) = -A_4(\omega,t).$$

2. $\pi^0 \to \gamma\gamma$ anomaly graph

$$A_8(\omega,t) = \frac{g_A}{(2\pi f_\pi)^2}\frac{2\mathcal{Z}-1}{t - m_{\pi^0}^2}; \quad A_1, \ldots, A_7 = 0. \tag{A2}$$

3. Δ *s* channel

$$A_1(\omega,t)=F(\omega,\Delta)\Big\{\tfrac{2}{3}(\omega^2+\tfrac{1}{2}t)(2+\Delta)G_M^2-\tfrac{2}{3}\omega^2\Delta G_E^2 + \frac{2}{3}\omega^3(G_M^2+G_E^2-G_MG_E)+\tfrac{1}{8}t^2G_M^2 + \omega t[(2+\tfrac{5}{6}\Delta+\tfrac{7}{6}\omega+\tfrac{1}{4}t)G_M^2-\tfrac{1}{6}(2+\Delta + \omega)G_MG_E+\tfrac{1}{6}\omega G_E^2]\Big\},$$

$$A_2(\omega,t)=F(\omega,\Delta)\{-\tfrac{2}{3}(2+\Delta)G_M^2-\tfrac{1}{3}\omega[(8+3\Delta)G_M^2 + 2\Delta G_E^2-(2+\Delta)G_MG_E]+\omega^2(-\tfrac{7}{6}G_M^2+\tfrac{5}{6}G_E^2 + \tfrac{2}{3}G_MG_E)+t[-\tfrac{1}{12}(1-\Delta)G_M^2-\tfrac{1}{12}\Delta G_E^2 + \tfrac{1}{3}\omega(-\tfrac{1}{2}G_M^2+G_E^2+\tfrac{5}{4}G_MG_E)+\tfrac{1}{32}t(G_M + G_E)^2]\},$$

$$A_3(\omega,t)=F(\omega,\Delta)\{-\tfrac{1}{3}\omega^2[2G_M^2+\Delta(G_M^2-G_E^2)] -\tfrac{1}{3}\omega^3(G_M^2+G_E^2-4G_MG_E)+t[-\tfrac{1}{6}(2+\Delta)G_M^2 + \tfrac{1}{3}\omega G_M(G_M(\tfrac{3}{2}+\Delta)+G_E(2+\Delta))+\omega^2(\tfrac{11}{12}G_M^2 - \tfrac{1}{12}G_E^2+\tfrac{1}{3}G_MG_E)+\tfrac{1}{4}tG_M^2(\tfrac{1}{2}+\omega)]\},$$

$$A_4(\omega,t)=F(\omega,\Delta)\{-\tfrac{1}{3}(2+\Delta)G_M(G_M+\omega G_E) -\omega(1+\tfrac{1}{3}\Delta)G_M^2+\tfrac{1}{3}\omega^2(G_M^2+G_E^2-G_MG_E) +\tfrac{1}{2}tG_M^2(\tfrac{1}{2}+\omega)\}, \quad \text{(A3)}$$

$$A_5(\omega,t)=F(\omega,\Delta)\{\tfrac{1}{3}(2+\Delta)G_M^2-\tfrac{1}{6}\omega[2(1+\Delta)G_M^2-\Delta G_E^2 +(2+\Delta)G_MG_E]-\omega^2G_M(G_M-G_E)+\tfrac{1}{4}t[G_MG_E +\tfrac{1}{2}\Delta G_M(G_M+G_E)-\omega G_M(G_M-G_E)]\},$$

$$A_6(\omega,t)=F(\omega,\Delta)\{\omega G_M[G_M+\tfrac{1}{2}\Delta(G_M+G_E)] +\omega^2G_M(G_M-G_E)+\tfrac{1}{4}t[G_M^2+\tfrac{1}{2}\Delta G_M(G_M+G_E) +\omega G_M(G_M-G_E)]\},$$

$$A_7(\omega,t)=F(\omega,\Delta)\{(2+\Delta)(\tfrac{7}{12}G_M^2+\tfrac{1}{2}G_MG_E)-\tfrac{1}{12}\Delta G_E^2 +\omega(\tfrac{7}{12}G_M^2-\tfrac{5}{12}G_E^2-\tfrac{1}{3}G_MG_E)-\tfrac{1}{16}t(G_M + G_E)^2\},$$

$$A_8(\omega,t)=F(\omega,\Delta)\{\tfrac{4}{3}(2+\Delta)G_M^2+\omega[4(1+\tfrac{1}{3}\Delta)G_M^2 -\tfrac{2}{3}(2+\Delta)G_MG_E]+\tfrac{1}{6}\omega^2(G_M^2+G_E^2-4G_MG_E) -\tfrac{1}{2}tG_M^2(\tfrac{1}{2}+\omega)\},$$

with $G_{M,E}=(3/2)g_{M,E}/(2+\Delta)$ and

$$F(\omega,\Delta)=-\frac{2}{3}\frac{1}{s-M_\Delta^2+iM_\Delta\Gamma(s)} =-\frac{2}{3}\frac{1}{2\omega-\Delta(2+\Delta)+iM_\Delta\Gamma(\omega)}. \quad \text{(A4)}$$

Here $\frac{2}{3}=T_3^\dagger T_3$ is the isospin factor, and the width Γ is given by Eq. (42).

The corresponding *u*-channel graphs are obtained by crossing, so that the crossing-symmetric amplitude is given by

$$A_i(\omega,t)+A_i(-\omega',t) \quad \text{for} \quad i=1,2,8;$$

$$A_i(\omega,t)-A_i(-\omega',t) \quad \text{for} \quad i=3,\ldots,7;$$

with $\omega'=p\cdot q'=(1-u)/2$.

4. HBχPT πN loops

Defining $\zeta=(\sqrt{s}-M_N)/m_\pi$ and $\tau=-2\zeta^2(1-\cos\theta)$, where θ is the center-of-mass angle between the incoming and outgoing photon momenta, one finds [19]

$$A_1(s,t)=-\frac{g_A^2m_\pi}{8\pi f_\pi^2}\Big\{1-\sqrt{1-\zeta^2}+\frac{2-\tau}{\sqrt{-\tau}} \times\Big[\frac{1}{2}\arctan\frac{\sqrt{-\tau}}{2}-I_1(\zeta,\tau)\Big]\Big\},$$

$$A_2(s,t)=-\frac{g_A^2}{8\pi f_\pi^2m_\pi}\frac{2-\tau}{(-\tau)^{3/2}}[I_1(\zeta,\tau)-I_2(\zeta,\tau)],$$

$$A_3(s,t)=\frac{g_A^2m_\pi}{8\pi^2f_\pi^2}\Big[\frac{1}{\zeta}\arcsin^2\zeta-\zeta+2\zeta^4\sin^2\theta I_3(\zeta,\tau)\Big],$$

$$A_4(s,t)=\frac{g_A^2}{4\pi^2f_\pi^2m_\pi}I_4(\zeta,\tau),$$

$$A_5(s,t)=-\frac{g_A^2}{8\pi^2f_\pi^2m_\pi}[I_5(\zeta,\tau)-2\zeta^2\cos\theta I_3(\zeta,\tau)],$$

$$A_6(s,t)=\frac{g_A^2}{8\pi^2f_\pi^2m_\pi}[I_5(\zeta,\tau)-2\zeta^2I_3(\zeta,\tau)]. \quad \text{(A5)}$$

Here

$$I_1(\zeta,\tau)=\int_0^1dz\,\arctan\frac{(1-z)\sqrt{-\tau}}{2\sqrt{1-\zeta^2z^2}},$$

$$I_2(\zeta,\tau)=\int_0^1dz\frac{2(1-z)\sqrt{-\tau(1-\zeta^2z^2)}}{4(1-\zeta^2z^2)-\tau(1-z)^2},$$

$$I_3(\zeta,\tau)=\int_0^1 dx\int_0^1 dz\frac{x(1-x)z(1-z)^3}{S^3}\left[\arcsin\frac{\zeta z}{R}+\frac{\zeta z S}{R^2}\right],$$

$$I_4(\zeta,t)=\int_0^1 dx\int_0^1 dz\frac{z(1-z)}{S}\arcsin\frac{\zeta z}{R},$$

$$I_5(\zeta,t)=\int_0^1 dx\int_0^1 dz\frac{(1-z)^2}{S}\arcsin\frac{\zeta z}{R}, \qquad \text{(A6)}$$

with

$$S=\sqrt{1-\zeta^2 z^2-\tau(1-z)^2 x(1-x)},$$

$$R=\sqrt{1-\tau(1-z)^2 x(1-x)}. \qquad \text{(A7)}$$

APPENDIX B: RESULTS FOR POLARIZABILITIES

The nucleon electric (α_N) and magnetic (β_N) polarizabilities:

$$\alpha_N=\frac{\alpha}{2}\frac{\partial^2}{\partial\omega^2}A_1^{(NB)}(0,0)+\alpha A_2^{(NB)}(0,0)$$

$$=\frac{5\pi\alpha}{6m_\pi}\left(\frac{g_A}{4\pi f_\pi}\right)^2-\frac{2\alpha g_E^2}{(M_N+M_\Delta)^3},$$

$$\beta_N=-\alpha A_2^{(NB)}(0,0)=2\alpha\frac{\partial}{\partial t}A_1^{(NB)}(0,0)$$

$$=\frac{\pi\alpha}{12m_\pi}\left(\frac{g_A}{4\pi f_\pi}\right)^2+\frac{2\alpha g_M^2}{(M_N+M_\Delta)^2\Delta}, \qquad \text{(B1)}$$

where $A_i^{(NB)}$ are the amplitudes with the Born graphs subtracted.

[1] E.L. Hallin *et al.*, Phys. Rev. C **48**, 1497 (1993).
[2] B.E. MacGibbon, G. Garino, M.A. Lucas, A.M. Nathan, G. Feldman, and B. Dolbilkin, Phys. Rev. C **52**, 2097 (1995).
[3] G. Blanpied *et al.*, LEGS Collaboration, Phys. Rev. Lett. **76**, 1023 (1996); **79**, 4337 (1997).
[4] G. Blanpied *et al.*, Phys. Rev. C **64**, 025203 (2001).
[5] V. Olmos de Leon *et al.*, Eur. Phys. J. A **10**, 207 (2001).
[6] M. Lucas, Ph.D. thesis, University of Illinois, 1994.
[7] D.L. Hornidge *et al.*, Phys. Rev. Lett. **84**, 2334 (2000).
[8] M. Lundin *et al.*, nucl-ex/0204014.
[9] N.R. Kolb *et al.*, Phys. Rev. Lett. **85**, 1388 (2000).
[10] K. Kossert *et al.*, Phys. Rev. Lett. **88**, 162301 (2002); nucl-ex/0210020.
[11] A.I. L'vov, V.A. Petrun'kin, and M. Schumacher, Phys. Rev. C **55**, 359 (1997).
[12] D. Drechsel, M. Gorchtein, B. Pasquini, and M. Vanderhaeghen, Phys. Rev. C **61**, 015204 (2000).
[13] V. Pascalutsa and O. Scholten, Nucl. Phys. **A591**, 658 (1995); O. Scholten, A.Y. Korchin, V. Pascalutsa, and D. Van Neck, Phys. Lett. B **384**, 13 (1996).
[14] T. Feuster and U. Mosel, Phys. Rev. C **59**, 460 (1999); G. Penner and U. Mosel, nucl-th/0207069.
[15] S. Kondratyuk and O. Scholten, Phys. Rev. C **64**, 024005 (2001); **65**, 038201 (2002).
[16] D. Babusci, G. Giordano, and G. Matone, Phys. Rev. C **55**, 1645 (1997).
[17] J.A. McGovern, Phys. Rev. C **63**, 064608 (2001).
[18] V. Bernard, N. Kaiser, and U.-G. Meißner, Nucl. Phys. **B383**, 442 (1992); V. Bernard, N. Kaiser, J. Kambor, and U.-G. Meißner, *ibid.* **B388**, 315 (1992).
[19] V. Bernard, N. Kaiser, and U.G. Meißner, Int. J. Mod. Phys. E **4**, 193 (1995).
[20] S.R. Beane, M. Malheiro, J.A. McGovern, D.R. Phillips, and U. van Kolck, nucl-th/0209002.
[21] M.N. Butler and M.J. Savage, Phys. Lett. B **294**, 369 (1992); M.N. Butler, M.J. Savage, and R.P. Springer, Nucl. Phys. **B399**, 69 (1993).
[22] V. Bernard, N. Kaiser, U.G. Meißner, and A. Schmidt, Z. Phys. A **348**, 317 (1994).
[23] T.R. Hemmert, B.R. Holstein, and J. Kambor, Phys. Rev. D **55**, 5598 (1997).
[24] T.R. Hemmert, B.R. Holstein, and J. Kambor, Phys. Lett. B **395**, 89 (1997); J. Phys. G **24**, 1831 (1998).
[25] T.R. Hemmert, B.R. Holstein, J. Kambor, and G. Knochlein, Phys. Rev. D **57**, 5746 (1998).
[26] H.W. Grießhammer, T.R. Hemmert, R. Hildebrandt, and B. Pasquini (unpublished).
[27] V. Pascalutsa, Phys. Rev. D **58**, 096002 (1998).
[28] V. Pascalutsa and R. Timmermans, Phys. Rev. C **60**, 042201(R) (1999).
[29] E. Jenkins and A.V. Manohar, Phys. Lett. B **255**, 558 (1991).
[30] H.F. Jones and M.D. Scadron, Ann. Phys. (N.Y.) **81**, 1 (1973).
[31] V. Pascalutsa, Phys. Lett. B **503**, 85 (2001).
[32] J.W. Chen, H.W. Griesshammer, M.J. Savage, and R.P. Springer, Nucl. Phys. **A644**, 245 (1998); H.W. Griesshammer and G. Rupak, Phys. Lett. B **529**, 57 (2002).
[33] R. Flores-Mendieta, C.P. Hofmann, E. Jenkins, and A.V. Manohar, Phys. Rev. D **62**, 034001 (2000); T.D. Cohen, Rev. Mod. Phys. **68**, 599 (1996); T.D. Cohen and W. Broniowski, Phys. Lett. B **292**, 5 (1992); W. Broniowski and T.D. Cohen, Phys. Rev. D **47**, 299 (1993); T.D. Cohen, hep-ph/0210278.
[34] F.E. Low, Phys. Rev. **96**, 1428 (1954); M. Gell-Mann and M.L. Goldberger, *ibid.* **96**, 1433 (1954).
[35] T. Becher and H. Leutwyler, Eur. Phys. J. C **9**, 643 (1999).
[36] E. Oset, E. Marco, J.C. Nacher, J.A. Oller, J.R. Pelaez, A. Ramos, and H. Toki, Prog. Part. Nucl. Phys. **44**, 213 (2000); U.G. Meissner and J.A. Oller, Nucl. Phys. **A673**, 311 (2000); A. Gomez Nicola, J. Nieves, J.R. Pelaez, and E. Ruiz Arriola, Phys. Lett. B **486**, 77 (2000).
[37] M.F. Lutz and E.E. Kolomeitsev, Nucl. Phys. **A700**, 193 (2002).
[38] K. Torikoshi and P.J. Ellis, nucl-th/0208049.
[39] Particle Data Group, Phys. Rev. D **66**, 010001 (2002).

[40] N. Fettes and U.G. Meissner, Nucl. Phys. **A679**, 629 (2001).
[41] C.W. Kao and T.D. Cohen, Phys. Rev. C **60**, 064619 (1999).
[42] H.W. Grießhammer, T. Hemmert, V. Pascalutsa, and D.R. Phillips (unpublished).
[43] C. Ordonez, L. Ray, and U. van Kolck, Phys. Rev. C **53**, 2086 (1996).
[44] E. Epelbaum, W. Glockle, and U.G. Meissner, Nucl. Phys. **A671**, 295 (2000).
[45] D.R. Entem and R. Machleidt, Phys. Lett. B **524**, 93 (2002).
[46] J.A.M. Vermaseren, computer code FORM, version 2 (Computer Algebra Nederland, Amsterdam, 1991).